Impact of pseudo-uridylation, substrate fold and degradosome organization on the endonuclease activity of RNase E

Md. Saiful Islam[1], Katarzyna J. Bandyra[1], Yanjie Chao[2,4], Jörg Vogel[2,3] and Ben F. Luisi[1,*]

[1]Department of Biochemistry, University of Cambridge, Tennis Court Road, Cambridge CB2 1GA, U.K.

[2]RNA Biology Group, Institute of Molecular Infection Biology, University of Würzburg, D-97080 Wurzburg, Germany

[3]Helmholtz Institute for RNA-based Infection Research (HIRI), Helmholtz Centre for Infection Research (HZI), Würzburg, Germany

[4]The Center for Microbes, Development and Health (CMDH), Institut Pasteur of Shanghai, Chinese Academy of Sciences, 320 Yue-yang Rd, Xuhui district, Shanghai, 200031, China

*correspondence: bfl20@cam.ac.uk

Running Title: *Mechanistic insights into activity of RNase E*

ABSTRACT

The conserved endoribonuclease RNase E dominates the dynamic landscape of RNA metabolism and underpins control mediated by small regulatory RNAs in diverse bacterial species. We explored the enzyme's hydrolytic mechanism, allosteric activation, and interplay with partner proteins in the multi-component RNA degradosome assembly of *Escherichia coli*. RNase E cleaves single-stranded RNA with preference to attack the phosphate located at the 5′ nucleotide preceding uracil, and we corroborate key interactions that select that base. Unexpectedly, RNase E activity is impeded strongly when the recognised uracil is isomerised to 5-ribosyluracil (pseudouridine), from which we infer the detailed geometry of the hydrolytic attack process. Kinetics analyses support models for recognition of secondary structure in substrates by RNase E and for allosteric autoregulation. The catalytic power of the enzyme is boosted when it is assembled into the multi-enzyme RNA degradosome, most likely as a consequence of substrate capture and presentation. Our results rationalize the origins of substrate preferences of RNase E and illuminate its catalytic mechanism, supporting the roles of allosteric domain closure and cooperation with other components of the RNA degradosome complex.

Keywords: Modified RNA, riboregulation, RNA recognition, ribonuclease mechanism, pseudouridine, RNA degradosome

INTRODUCTION

RNase E, a key bacterial endoribonuclease of ancient evolutionary origin, has multifaceted activities critical to organism fitness, including the turnover of mRNA, maturation

of precursors of tRNA and rRNA, processing and degradation of small regulatory RNAs, and rRNA quality control (Mackie 2013, 1998; Bandyra et al. 2013). Once cleaved by RNase E, an mRNA becomes committed to an irreversible fate of rapid deconstruction; but at the same time, the enzyme can contribute to an orderly genesis of structured RNAs from precursors that circumvents destructive pathways, provided that those species satisfy quality control checks. The enzymatic activity of RNase E, which appears to be nuanced, serves as a key determinant of cellular RNA lifetime in cells. Its substrate preferences and encounter rate with RNA impact on transcript lifetime *in vivo* and are of interest for elaborating a potential code that could define cellular RNA fate.

Decades of analysis of RNase E activity indicate that there is no simple sequence code for its substrates *per se*, but instead a strong preference to cleave within single-stranded regions enriched in A or U (Chao et al. 2017; Del Campo et al. 2015; Kime et al. 2010, 2014; Mackie 2013). Global RNA target analyses performed both *in vivo* and *in vitro* identify uracil positioned to the 3′ side adjacent to the nucleotide of the scissile phosphate (the +2 position) as a strong signature for RNase E activity (Chao et al. 2017). For many substrates that follow either destructive and maturation pathways, the enzyme is activated by transformation of the 5′ end of the substrate from a triphosphate normally found on nascent transcripts, to a monophosphate found on processed species (Mackie 2013). For other substrates, the status of the 5′ end is not so critical for RNase E action (Baker and Mackie 2003; Clarke et al. 2014; Kime et al. 2014), and for these '5′ end bypass' substrates, other features such as secondary structure of the RNA appear to be important. Secondary structure contributes to recognition of sites for cleavage in both degradative and processing pathways (Richards and Belasco 2021; Bandyra et al. 2018; Updegrove et al. 2019).

The critical endonuclease activity of RNase E is encompassed within the highly conserved amino-terminal domain (NTD) (Figure 1a), which corresponds to roughly half the

protein mass. Crystallographic studies of this domain have provided insight into the origins of substrate recognition and 5′-end dependent activation (Callaghan et al. 2005; Bandyra et al. 2018; Koslover et al. 2008) (Figure 1a). Key structural motifs of the NTD include an RNA binding S1 domain and a 5′-sensor that can read the chemical status of the RNA 5′-end (Figure 1a). The recognition of the 5′-end triggers a conformational switch that maneuvers the S1 domain to clamp onto substrates and present them in the active site with geometry favorable for hydrolytic attack. A zinc-coordination motif links two protomers into a dimer, and two such dimers self-associate through a small domain that is evolutionarily related to the KH RNA binding module (Pereira and Lupas 2018) (Figure 1a). A vestigial RNase H-like subdomain has no catalytic activity but has been observed to cooperate with the KH-like small domain to recognize duplex structures in substrates and help present adjacent single-stranded regions to the proximal active site (Bandyra et al. 2018) (Figure 1a). Surprisingly, the enzyme is driven into a hyperactive state by simple substitutions in a conserved pocket of this domain that correspond to nearly single-atom replacement (D26N, D28N, D338N; hereafter NTD-3M) (Bandyra et al. 2018; Updegrove et al. 2019). These observations support a model in which the RNase H-like domain auto-regulates the activity of the enzyme by influencing the energetics of domain closure (Bandyra et al. 2018).

The carboxy-terminal half of the protein, which is predicted to be intrinsically disordered (Aït-Bara et al. 2015; Aït-Bara and Carpousis 2015; Callaghan et al. 2004), provides the scaffold to assemble protein partners into the RNA degradosome complex (Bruce et al. 2018; Bandyra et al. 2013, 2018). Through the cooperation of its components and recruitment of RNA chaperones such as Hfq, the RNA degradosome is the central machinery in *Escherichia coli* and many other species for processing of structured precursors and turnover of RNA. RNase E also contains a short amphipathic α-helical domain that interacts with the *E. coli* inner membrane, and the resulting membrane localisation of the degradosome adds a

spatial layer to post-transcriptional gene regulation (Khemici et al., 2008; Hadjeras et al. 2019; Mackie, 2013). Two RNA binding sites in the C-terminal domain of RNase E, referred to as AR1 and AR2, cooperate with the RNA helicase RhlB to assist in substrate unwinding and remodelling (Khemici and Carpousis 2004; Garrey et al. 2009; Leroy et al. 2002; Chandran et al. 2007). The two RNA binding sites, together with RhlB can interact with ribosomes (Tsai et al. 2012) and may enable the degradosome to cleave mRNA in support of a proposed scavenging process (Deana and Belasco 2005; Dreyfus 2009). A plausible scenario is that the close proximity of the RNA degradosome to the translational machine prevents the translation of aberrant transcripts and rescues stalled ribosomal assemblies as part of bacterial RNA surveillance.

Open questions remain regarding details of the RNase E catalytic mechanism, and its capacity to act on modified RNA. The effect of the interplay between the components of the degradosome on the quantitative activity of the catalytic domain also have not been evaluated. In this report, we measured the ribonuclease activity of RNase E and variants that effect substrate recognition, and we explored how the RNA degradosome assembly cooperates with this activity. Analysis of RNase E activity on substrates with pseudouridine shows that, surprisingly, the enzyme is very sensitive to this modification. Taken together, our results provide mechanistic insights into RNase E catalytic mechanism, allostery, and cooperation within the RNA degradosome complex.

RESULTS

K112 plays an important role in substrate preference and cleavage by RNase E

Modelling using the crystal structures of the N-terminal catalytic domain (NTD) of RNase E predicted that S1 domain residues K112 and F67 interact with the base at position +2

to orient the single stranded region of the RNA substrate into a favourable geometry at the active site for nucleophilic attack by water (Chao et al. 2017) (Figure 1a). Uracil at the +2 position is predicted to be favoured by a hydrogen bonding interaction between the amino group of K112 and the exocyclic carbonyl groups that contributes to the sequence preference at that position. Based on the x-ray structure of RNase E with modified RNA (Callaghan et al. 2005), the +2 base is also predicted to be sandwiched between the aromatic ring of F67 and the aliphatic component of the K112 side chain (Figure 1a). The orientation for the K112 side chain to make the base-sandwiching interaction may differ from that to make the hydrogen bond to U+2, and it may switch conformation during the catalytic process so that its amino group may interact with the phosphate to stabilise the charge of the hydrolytic intermediate.

To test the importance of K112, we compared activities of purified wild-type and mutant version of NTD using a model single-stranded RNA substrate composed of 20 adenine residues (A20) and its uracil variant with a single uracil at position 15 (A20U) (Figure 1b). The time course for the cleavage is shown in Figure 1b, with products resolved on an RNA denaturing gel. At the enzyme:substrate ratios used in these assay conditions, corresponding to multiple turnover conditions, RNase E NTD cleaves efficiently at the phosphate 2 nucleotides upstream of uridine, consistent with the U+2 ruler-and-cut mechanism (Chao et al. 2017). The cleavage rate of the uracil-containing substrate is higher compared to the substrate with no uracil (Figure 1b, top panel, compare A20 and A20U). When K112 is substituted with alanine, the enzyme activity and specificity are greatly diminished for the uracil-containing substrate, with more starting substrate remaining over the time course and the degradation pattern resembling a uniform ladder, as distinct from being enriched for a particular species (Figure 1b, middle panel, compare A20 and A20U with top panel). Even the comparatively conservative substitution of K112 with the long polar side chain of glutamine has diminished cleavage preference for the U+2 position (Figure 1b, bottom panel). In general, substitution of

lysine by the polar glutamine is expected to retain capacity for hydrogen bond formation. However, based on the crystal structure, the glutamine is predicted to be too short to hydrogen bond with either the uracil carbonyl groups or the phosphate backbone. These results corroborate the importance of the K112 interaction for catalysis and suggest that the hydrogen bonding interaction with either the uracil base or the scissile phosphate or both are required for optimal activity.

Pseudouridine impedes RNase E activity and shifts the cleavage site

The substitution of the uracil at position +2 with pseudouridine (Ψ) involves an isomeric transformation of the base and was not expected to impact the presentation of the hydrogen bonding groups of O2 and O4 (Figure 1c). However, pseudouridine showed a profound effect on the cleavage activity of RNase E (Figure 1b top panel, compare A20U with A20Ψ). Most of the pseudouridine containing substrate resisted cleavage by RNase E in the course of the experiment. The cleavage site seems to be shifted relative to the cleavage when uridine is present. These findings suggest that the recognition of uracil is not simply due to a hydrogen bonding interaction with the principal substituents of the base, but also depends on the detailed interactions that influence the phosphodiester geometry (Westhof 2019). The substitution of U with pseudouridine may affect the hydration pattern of the substrate and the energy required to achieve the conformation that enables development of the enzymatic transition state (Figure 1c) (Charette and Gray 2000).

The substitution of K112 with Q, which impedes activity of the wild-type enzyme, changed the cutting pattern of the pseudouridine containing substrate. The preferred cleavage site of the K112Q mutant protein moved to the position +2/+3 relative to the cut-site for the wild-type counterpart (Figure 1b, middle and bottom panels). A lesser degree of cleavage of

pseudouridine containing substrate was also observed for the K112Q mutant. The overall reduction in cleavage rate along with a shift in preferred cleavage site suggests that the activation of hydrolysis requires a long positively charged or polar side chain at position 112 (Figure 1a). The K112Q substitution perhaps causes the substrate to align differently in the active site pocket so that it is shifted by one or two nucleotides in the 3′ direction compared to the corresponding wild-type complex.

RNase E catalytic power can be boosted by substitutions at DNase I and RNase H-like domains

Earlier studies showed that the catalytic activity of RNase E is boosted by mutations of conserved, non-catalytic residues in the RNase H-like domain (D26N and D28N) and DNase I domain (D338N) (Figure 2a, right panel) (Bandyra et al. 2018). The substitutions are at a distance from the active site but involve regions where the conformational changes associated with apo to substrate-bound states occur and are likely to impact on the allosteric switching of the enzyme (Bandyra et al. 2018). We compared the catalytic activity of the wild type (NTD) and the hyperactive variant carrying mutations at positions D26, D28, and D338 where all three aspartate residues were mutated to asparagine (NTD-3M). For substrates, we used GlmZ, which is a regulatory sRNA that gets inactivated by RNase E cleavage, and 9S RNA which is a precursor of ribosomal 5S RNA (Figure 2a).

The enzyme cleaves the 9S mainly at three sites to form the p5S precursor ribosomal RNA product (Figure 2a) (Carpousis et al. 1994; Christiansen 1988; Cormack and Mackie 1992). Stem-loop II has previously been shown as the minimal structural requirement needed for RNase E to cleave at the '*a*' site (Figure 2a) (Mackie 2013; Cormack and Mackie 1992; Carpousis et al. 1994). We also generated three segments of 9S RNA encompassing different

predicted secondary structures (indicated by bars above the 9S schematic in Figure 2a). Version 1 has cut-sites '*a*' and '*b*' and is similar to the 9Sa substrate previously investigated by others (Carpousis et al. 1994). Version 2 has cut-sites '*a*' and '*c*', and version 3 encompasses only cut-site '*b*' (Christiansen 1988). The cleavage assays with 9S and its truncated versions confirm earlier observations (Carpousis et al., 1994; Mackie and Genereaux, 1993) that RNase E action can be influenced by the secondary structures upstream and downstream to the recognition site (Figure 2c, left panel).

Compared to the wild-type enzyme, NTD-3M showed higher activity for all substrates tested. Its activity is shown for the 9S substrate in Figure 2b, for the three smaller constructs of 9S in Figure 2c, and for the GlmZ sRNA in Figure 2d. These results suggest that the activity enhancement of NTD-3M does not require a specific sequence or RNA fold. GlmZ cleavage by RNase E is guided by the protein RapZ, which has high specificity for the guiding effect and is not observed with the RNA chaperone Hfq (Figures 2e and S1) (Gonzalez et al. 2017; Durica-Mitic and Görke 2019; Kalamorz et al. 2007; Urban and Vogel 2008; Göpel et al. 2013). In the presence of NTD-3M, the guiding effect of RapZ is enhanced, but the GlmZ cleavage is either inhibited or proceeds non-specifically without forming GlmZ-Pro in the presence of Hfq (Figure 2e).

The 5′ phosphorylation state of 9S RNA can impact on the first cleavage events, with the second event having the activating 5′P group present and anticipated to be intrinsically accelerated if the group is read by the enzyme (Mackie 2013; Cormack and Mackie 1992). For the 9S substrate, the status of the 5′ end affects the rate disappearance of the 9S band and generation of the p5S product (graphs in lower panel, Figure 2b), with a boost seen for 5′ monophosphate versus triphosphate, corroborating earlier findings that 5′-sensing can contribute to the first cleavage event in 9S processing by RNase E (Mackie 2013; Cormack

and Mackie 1992). This boosting effect is also seen for the NTD-3M mutant and suggests that the mutation does not impact on 5′ sensing.

For all substrates tested, a boost in catalytic power was observed, due to both increased catalytic rate and decreased K_m (Table 1). Taken together, these results support the proposed role of allosteric autoregulation of enzyme activity (Bandyra et al. 2018), in which domain closure helps to pre-organize the active site so that the apparent affinity of the Michaelis-Menten complex increases probably by decreasing the energy barrier to capture and engulf the substrate.

Metals in the catalytic mechanism: RNase E active site may recruit one metal in the apo form

The active site bears two conserved aspartate residues (D303 and D346) that recruit magnesium ion to activate a water molecule for nucleophilic attack on the scissile phospho-diester bond (Thompson et al. 2015; Callaghan et al. 2005) (Figure 1a). One question relevant to the mechanism is whether metal is bound to the site in the apo form or if metal binding requires substrate. The binding interactions between RNase E and metal cofactor was evaluated by isothermal calorimetry (ITC) using a variant of RNase E with residue D346 replaced with a cysteine residue, which was reported previously to be catalytically active in presence of Mn^{++}, but not Mg^{++} (Figure 3a) (Thompson et al. 2015). Testing the activity of NTD.D346C on two different RNAs, 9S and the small RNA RprA, confirms that the enzyme is active for cleavage only in the presence of Mn^{++} (Figure 3b and 3c). Using isothermal titration calorimetry (ITC) and titrating the mutant enzyme against Mn^{++} yields a K_D for metal binding in the absence of RNA at 17 μM, with associated ΔH = -19.45 kcal/mol and ΔS = -35.4 cal/mol/deg (Figure 3d).

The binding profile indicates that one metal ion can be bound by each subunit of the catalytic domain in the absence of substrate.

Probing RNase E mechanism with unnatural amino acids

To further explore interactions between the catalytic NTD and its substrates, we prepared derivatives of the protein with the photo-crosslinkable amino acid para-azido-phenylalanine (p-AzidoPhe) incorporated at specific positions in the 5′-sensing pocket and the duplex-RNA binding site using the amber suppressor system (Chatterjee et al. 2014) (Figure 4a). Single substitutions were made at residues M130, I139, R142 in the 5′-sensing pocket and Y269 on the duplex binding surface (Figure 4b). Surprisingly, time course activity assays indicated that formation of the p5S species from 9S becomes impeded by all three substitutions in the 5′-sensing pocket, suggesting that the changes perturb RNA interactions (Figure 4c). On the other hand, the Y269 substitution at the duplex binding surface showed little impact on activity (Figure 4c). Exposing NTD p-AzidoPhe derivatives to light at 254 nm in the presence of the 9S segments indicated schematically in Figure 2a did not yield photo-crosslinking directly to the RNA that could be detected by mobility shifts in denaturing protein gels (Figure 4d). However, the protein migrated differently in the denaturing gel upon UV light illumination in the absence of RNA, and this may arise from intra-molecular crosslinks or masking of sites by the bound RNA (Figure 4d). While these results did not yield the RNA-protein adducts that were anticipated, they demonstrate the feasibility of introducing unnatural amino acids into RNase E for future studies and also highlight the sensitivity of the 5′-sensing pocket to mutations that impact on processing activity.

Activities of the degradosome for cleavage of complex substrates

To explore how RNase E activity is impacted by the degradosome organization, we studied the activity of the assembly to cleave 9S and GlmZ. Purified recombinant degradosome (comprising RNase E 1-1061, RhlB, enolase, and PNPase) was prepared, as well as a subassembly comprising RNase E 1-850, RhlB, and enolase (truncated degradosome; Figure 5a). The activity for processing of 9S was relatively greater for the truncated degradosome and full degradosome assemblies compared to the isolated catalytic domain under identical experimental conditions (Figure 5b, Table 1). The cleavage rates were also seen to be greater for 5′P-9S compared to 5′PPP-9S (Figure 5b). Increased activity was also observed for the 9S segments (Figure 5c) and processing of GlmZ (Figure 5d). As seen the results with the NTD, RapZ has a guiding effect on cleaving GlmZ, but Hfq does not (Figures 5e and supplementary Figure S1).

The degradosome shows increased catalytic power (k_{cat}/K_m) compared to the NTD for all substrates, mostly through changes to k_{cat} (Figure 5f, Table 1). The degradosome assembly has several RNA binding sites that may help to capture and channel substrates (Dendooven et al., 2021), perhaps combined with better organization of the RNase E active site that potentiates domain closure and ensuing catalytic activity.

DISCUSSION

In many bacterial species, the half-lives of most transcripts are defined by the activity of RNase E, and sequence and structural preferences for substrates have been identified from *in vitro* and *in vivo* experiments (Clarke et al. 2014; Kime et al. 2014; Chao et al. 2017; Mackie 2013). Here, we explored the activity of RNase E on different RNAs to gain further insight into substrate recognition and cooperation between domains and partner proteins. We quantified metal interaction and impact of allosteric mutations and degradosome assembly on

activity. The impact of substrate modification by pseudouridinylation had not been addressed in earlier studies and this was studied here.

The cleavage assays with 9S and truncated versions confirm that RNase E action can be influenced by secondary structures upstream and downstream of the cleavage site. Cleavage of all investigated RNAs is influenced by the RNA degradosome assembly. Corroborating earlier findings, mutations in the RNase H-like subdomain boosts hydrolytic activity (Bandyra et al. 2018). A higher reaction rate for the NTD-3M mutant with lower K_m and higher k_{cat} suggest that the RNase H-like and DNase I domains help to cleave RNAs by increasing the catalytic power of the enzyme. As these domains switch conformation with substrate binding, it is possible that they can impact on product release, with the mutant acting more quickly than wild type for this step.

The results presented here corroborate the importance of uracil at position +2 with respect to the cleavage site as a key feature of a preferred cleavage site by RNase E and the role of residue K112 in recognising the +2 uracil. Unexpectedly, cleavage by RNase E is strongly impeded when the +2 uracil is substituted with pseudouridine, which is surprising given that this substitution presents only one new hydrogen bonding group on the pyrimidine. The isomerisation of uracil to pseudouridine presents the N1 as a hydrogen bond donor and may affect the hydration pattern that will include interaction with the phosphate backbone. In most RNA structures, N1 is predicted to interact with the phosphate backbone of both the pseudouridine and the 5′ residue (Charette and Gray 2000; Westhoff, 2019). In the context of RNase E catalytic site, this interaction could restrict the backbone conformation at position +2 and disfavour the geometry necessary for catalysis.

Pseudouridine is a commonly occurring modification of tRNA and rRNA in all domains of life (Charette and Gray 2000). The modification of tRNA fragments with pseudouridine has been implicated in translation control in early stages of mammalian embryogenesis (Guzzi et

al. 2018). In *E. coli* and other bacteria, the precursors of tRNAs and rRNAs are matured by RNase E cleavage, and the enzyme contributes to quality control of rRNA (Sulthana et al. 2016). As part of the mechanism of quality control, RNase E could hypothetically sense whether the precursors have been properly modified with pseudouridine and destroy those that have not undergone the isomerization. However, our tests of RNase E activity on tRNAs isolated from cells that are deficient in pseudouridine synthase show that these species, as well as the wild type controls, are resistant to digestion (data not shown). Recent studies suggest that pseudouridine is also prevalent in mRNAs and noncoding RNAs, and that pseudo-uridylation is regulated by environmental stresses and nutrient availability (Carlile et al. 2014). Differential sensitivity of pseudouridine to ribonucleases may provide a new mechanism to control RNA stability and/or turnover. Lastly, the results presented here may offer a method to map pseudouridine positions in a sample of RNA through differential sequencing. For example, comparison of RNA sequencing of sample digested with wild type and mutant RNase E (K112A or K112Q) might reveal attenuation of signal for substrates with uridine at position +2, but a shift of signal to the -2 or -3 position in the presence of pseudouridine (Figure 6, right panel). This could help to pinpoint pseudouridine positions in denatured samples of cell-extracted RNA.

The degradosome scaffolding domain of RNase E is predicted to be natively unstructured, and this property has been highly sustained in evolution (Marcaida et al. 2006; Aït-Bara and Carpousis 2015). Recent findings indicate that the natively unstructured character may enable the degradosome to form microscopic condensates in the presence of RNA (Al-Husini et al. 2020, 2018), a property shared with many other RNA binding proteins from all domains of life (Lin et al. 2015; Boeynaems et al. 2018). Enzymatic activities can be concentrated within these bodies, and the environment can affect substrate RNA secondary structures (Guzikowski et al. 2019; Nott et al. 2015). The RNA degradosome from the aquatic

Gram-negative bacterium *Caulobacter crescentus* coalesces into nano-scale condensates upon RNA-binding, and these are reversed by RNA turnover (Al-Husini et al. 2020, 2018). Similarly, the membrane associated *E. coli* RNA degradosome forms transient clusters over the membrane during RNA turnover (Moffitt et al. 2016; Strahl et al. 2015).

The results presented here show that the catalytic power of RNase E is boosted when the enzyme is assembled into the multi-enzyme RNA degradosome assembly. Our observations suggest that the degradosome facilitates RNase E activity, and this may arise through substrate capture by the multiple RNA-binding sites in the assembly (Figure 6, left panel). The increase in catalytic power may also be allostery-mediated. We anticipate that the clustering of degradosomes in bodies with liquid-like phase separation further concentrates the enzymatic activities of the machinery and changes the physicochemical conditions that impact on activity. Our results rationalize the origins of substrate preferences of RNase E and illuminate its catalytic mechanism, supporting the roles of allosteric domain closure and cooperation with other components of the RNA degradosome complex.

Materials and methods

RNase E NTD expression and purification

RNase E (1-529) wild type and mutants were prepared as previously described (Callaghan et al. 2005; Bandyra et al. 2018). In brief, *Escherichia coli* strain BL21(DE3) was transformed with vector pET16 expressing RNase E (1-529) with an *N*-terminal his_6-tag. Cultures were grown in 2xTY media supplemented with 100 µg/mL carbenicillin at 37ºC, in an orbital shaker set at 220 rpm. The culture was induced between 0.5 to 0.6 OD_{600nm} by adding 1 mM isopropyl-β-thiogalactopyranoside (IPTG) and harvested after 3 hours of incubation by centrifugation at

4200 *g* and 4º C for 30 minutes. Cell pellets were stored as suspension in nickel-column buffer A (20 mM Tris pH 7.9, 500 mM NaCl, 5 mM imidazole, 1 mM $MgCl_2$) at -80ºC. Once thawed, the cell culture suspension was supplemented with DNase I and EDTA-free protease inhibitor cocktail tablet (Roche) and cells were lysed by passing through an EmulsiFlex-05 cell disruptor (Avestin) for 2-3 times at 10-15 kbar pressure. The lysate was clarified by centrifugation at 35000 *g* for 30 minutes at 4º C and the supernatant was loaded onto a pre-equilibrated HiTrap Chelating HP column charged with nickel ions (GE Healthcare). The column was washed extensively with wash buffer (20 mM Tris pH 7.9, 500 mM NaCl, 100 mM imidazole, 1 mM $MgCl_2$), followed by linear-gradient elution of RNase E with elution buffer (20 mM Tris pH 7.9, 500 mM NaCl, 500 mM imidazole, 1 mM $MgCl_2$). Fractions containing RNase E were pooled and loaded on a butyl sepharose HP column (GE Healthcare) which previously was equilibrated in high-salt buffer (50 mM Tris pH 7.5, 50 mM NaCl, 25 mM KCl, 1 M $(NH)_2SO_4$). A gradient of a low-salt buffer (50 mM Tris pH 7.5, 50 mM NaCl, 25 mM KCl, 5% glycerol) was used to elute protein. Fractions containing RNase E were pooled, concentrated and loaded onto a size-exclusion column (Superdex^{TM} 200 Increase 10/300, GE Healthcare) equilibrated previously in storage buffer (20 mM HEPES pH 7.5, 500 mM NaCl, 10 mM $MgCl_2$, 0.5 mM TCEP, 0.5 mM EDTA, 5% glycerol). The optimal fractions were flash frozen in liquid nitrogen and stored at -80 °C until further use.

RNase E NTD azido-phenylalanine incorporation and purification

An amber suppressor codon (TAG) was inserted by site-directed mutagenesis at defined positions of the gene encoding RNase E NTD in the pET16 expression plasmid described in the previous section. The sequences of the primers used to insert TAG codons are provided in Table 2. Para-azido-phenylalanine (p-AzidoPhe) was inserted in RNase E NTD by co-

expressing in *Escherichia coli* BL21(DE3) the pET16 carrying mutated *rne* genes and pDULE2 carrying genes encoding for an orthogonal tRNA synthetase (Chatterjee et al. 2014).

Cultures of transformed cells were grown in LB medium supplemented with carbenicillin (100 µg/mL), spectinomycin (40 µg/mL), arabinose (0.05% w/v), and p-AzidoPhe (1 mM) at 37 °C and 220 rpm. Cultures were induced between 0.5 to 0.6 OD_{600nm} by IPTG and cells were harvested by following the same procedure as used for NTD. P-AzidoPhe derivatives of NTD were purified by following the same procedure as used for NTD. The IMAC binding buffer was composed of 50 mM phosphate buffer pH 7.9, 500 mM NaCl, 5 mM imidazole, 1 mM $MgCl_2$, with elution buffer containing 500 mM imidazole. The size-exclusion buffer was composed of 50 mM phosphate buffer pH 7.5, 500 mM NaCl, 10 mM $MgCl_2$, 0.5 mM EDTA, 5% glycerol.

The p-azido phenylalanine incorporation was confirmed by biotinylation of azido group using EZ-link Phosphine-PEG3-Biotin (Thermo Fisher) (Agard et al. 2006; Saxon and Bertozzi 2000). Briefly, 50 µM of azido phenylalanine derivatives of RNase E NTD was reacted with 1 mM EZ-link Phosphine-PEG3-Biotin (x20 excess) at room temperature for 20 hrs. This allowed the phosphine group of EZ-link Phosphine-PEG3-Biotin to react with the azido group of p-azido phenylalanine, producing an aza-ylide intermediate (the Staudinger Reaction) (Saxon and Bertozzi 2000). Unbound biotin was removed by buffer exchange into phosphate buffered saline by using Micro BioSpin-6 column concentrator, followed by concentrating to 50 µL. Samples were then loaded on SDS-PAGE gel and p-azido phenyl alanine was detected against anti-Biotin using a Western blot transfer protocol and enhanced chemiluminescence. Similar experiment was carried out with addition of reducing agent in the phosphate buffered saline, resulting in a less intense band. While p-azido phenyl alanine derivatives showed band corresponding to NTD, the wild type NTD control did not show any band with the same procedure.

Expression and purification of truncated degradosome

E. coli strain ENS134-10 was used to express RNase E 1-850 and full-length RhlB genes from the expression vector pRSF-DUET and full-length enolase from pET21b. Bacterial cultures, supplemented with 15 µg/mL kanamycin and 25 µg/mL carbenicillin, were grown at 37º C until the OD_{600} reached 0.3-0.4 when protein production was induced by adding 1 mM IPTG. After overnight growth at 18º C, cells were harvested by centrifugation at 4200 g, 4º C for 30 minutes. Cells were resuspended in nickel-column buffer A (50 mM Tris pH 7.5, 1 M NaCl, 100 mM KCl, 5 mM imidazole, 10 mM $MgCl_2$, 0.02% n-dodecyl β-D-maltoside (β-DDM) and stored at -80° C until further use. Once thawed, the cells were supplemented with cOmplete EDTA-free protease inhibitor tablet (Roche), 1% Triton X-100, 1 mM TCEP, 1 mM PMSF, and 100 units of DNase I. Cells were lysed by passing the suspension through an EmulsiFlex-05 cell disruptor (Avestin) for 2-3 times at 10-15 kbar pressure. The lysate was clarified by centrifugation at 35000 g for 30 minutes and the supernatant was loaded onto a pre-equilibrated HiTrap Chelating HP column charged with nickel ions (GE Healthcare). The column was washed extensively with wash buffer (50 mM Tris pH 7.5, 1 M NaCl, 100 mM KCl, 100 mM imidazole, 10 mM $MgCl_2$, 0.02% β-DDM), followed by elution of truncated degradosome by a linear gradient of elution buffer (50 mM Tris pH 7.5, 1 M NaCl, 100 mM KCl, 500 mM imidazole, 10 mM $MgCl_2$, 0.02% β-DDM). Enriched fractions evaluated by SDS-PAGE were pooled together and passed through a cation exchange column (SP HP, GE Healthcare) which previously was equilibrated in a low-salt buffer (50 mM Tris pH 7.5, 50 mM NaCl, 10 mM KCl, 0.02% β-DDM). A linear gradient (0-50%) with a high-salt buffer (50 mM Tris pH 7.5, 2 M NaCl, 10 mM KCl, 0.02% β-DDM) was used to elute truncated degradosome. Desired fractions were pooled together, concentrated using 100 kDa molecular weight cut-off concentrator and loaded onto a Superose6 10/300 size-exclusion column (GE Healthcare) equilibrated previously in storage buffer (50 mM HEPES pH 7.5, 400 mM NaCl, 100 mM KCl,

5 mM DTT, 0.02% β-DDM). Fractions containing the degradosome complex were flash frozen in liquid nitrogen and stored at -80 °C until further use.

Expression and purification of full degradosome

Escherichia coli strain NCM3416 with a chromosomally strep-tagged RNase E was used to express the endogenous full-length RNA degradosome. Bacterial cultures were grown at 37º C in 2xYT media supplemented with 50 µg/mL kanamycin until the OD_{600} reached to 2.0 when protein production was induced by adding 1 mM IPTG. After overnight growth at 18º C, cells were harvested by centrifugation at 5020 g, 4º C for 30 minutes. Cells were resuspended in strep buffer A (50 mM Tris pH 7.5, 1 M NaCl, 100 mM KCl, 10 mM $MgCl_2$, 0.02% β-DDM) and stored at -80° C until further use. Once thawed, the cells were supplemented with cOmplete EDTA-free protease inhibitor table (Roche), 1% Triton X-100, 1 mM TCEP, 1 mM PMSF, 100 units of DNase I, and 1 mg/mL lysozyme (Sigma). Cells were lysed by passing the suspension through an EmulsiFlex-05 cell disruptor (Avestin) for 2-3 times at 10-15 kbar pressure. The lysate was clarified by centrifugation at 35000 g for 30 minutes and the supernatant was passed through a 0.45 µ membrane filter before loading onto a pre-equilibrated HiTrapHP Strep column (GE Healthcare). The column was washed extensively with strep Buffer A before the endogenous RNA degradosome was step-eluted with a strep buffer B (50 mM Tris pH 7.5, 200 mM NaCl, 100 mM KCl, 10 mM $MgCl_2$, 0.02% β-DDM), followed by elution of full degradosome by elution buffer (50 mM Tris pH 7.5, 1 M NaCl, 100 mM KCl, 500 mM imidazole, 10 mM $MgCl_2$, 0.02% β-DDM, 2.5 mM desbiotin(Sigma)). The best fractions were pooled and applied to a cation exchange column (HiTrap Heparin HP, GE Healthcare) equilibrated in a low-salt buffer (50 mM Tris pH 7.5, 50mM NaCl, 10 mM KCl, 0.02% β-DDM). A linear gradient (0-50%) with high-salt buffer (50 mM Tris pH 7.5, 2 M NaCl, 10 mM KCl, 0.02% β-DDM) was used to elute the full degradosome. Based on the purity

of the eluted fractions, desired fractions were pooled together, concentrated down using 100 kDa MWCO concentrator and loaded onto a Superose6 10/300 size-exclusion column (GE Healthcare) equilibrated previously in storage buffer (50 mM HEPES pH 7.5, 400mM NaCl, 100 mM KCl, 5 mM DTT, 0.02% β-DDM). Desired fractions were flash frozen in liquid nitrogen and stored at -80 °C until further use.

RNA preparation by *in vitro* transcription

RNAs were prepared by *in vitro* transcription. Plasmids with the 9S, RprA and GlmZ RNA genes were generously provided by A.J. Carpousis (CNRS, Toulouse), Kai Papenfort (Jena) and Boris Görke (Vienna), respectively. First, genes were amplified by PCR using primers which were also adding T7 promoter. Next, RNA was synthesized from the PCR amplified product using T7 RNA polymerase at 37º C, followed by treating the reaction mixture with TURBO DNase for 15-20 minutes at 37º C. Finally, the RNA was purified by urea-PAGE followed by electroelution at 4º C and 100V (EluTrap, Whatman)(Bandyra et al. 2018). In order to generate 5'-monophosphorylated RNA, rGMP was used in addition to rGTP (5:1 molar ratio) while keeping other reaction component and purification steps same as before (Bandyra et al. 2018). For all RNAs, purity was checked in 8% urea-PAGE gel stained with SYBRgold RNA dye (Thermo Fisher).

RNA degradation assays with pseudouridine substrates

20-mer poly-adenine (A20), poly-adenine with an uracil residue at position 15 (A20U) and poly-adenine with a pseudouridine residue at position 15 (A20Ψ) were obtained from Dharmacon. Oligoribonucleotides were 5′ labelled with ^{32}P using polynucleotide kinase (Fermentas), according to manufacturer instructions. Assays were carried out in reaction buffer

(25 mM Tris-HCl pH 7.5, 50 mM NaCl, 50 mM KCl, 10 mM $MgCl_2$, 1 mM DTT, 0.5 U/µL RNase OUT) at 37°C. 100 nM purified RNase E NTD was used for the reactions. Time course reactions were stopped at indicated time points by addition of STOP solution (20 mM EDTA, 2% w/v SDS). RNA loading dye (Thermo Fisher) was added to samples which were denatured (98°C, 2 min) and loaded onto polyacrylamide gels containing 7.5 M urea. Gels were dried and exposed to phosphor screens (GE Healthcare) and the signal analysed with TyphoonT 9400 (GE Healthcare).

Kinetics assay

Ribonuclease cleavage of RNAs by RNase E was carried out at 30º C in the reaction buffer as above (Bandyra et al. 2018). In case of time course assay, samples were quenched at a predetermined time points by adding proteinase K mix (proteinase K in proteinase K buffer of 100 mM Tris-HCl pH 7.5, 150 mM NaCl, 12.5 mM EDTA, 1% SDS), followed by incubation at 50º C for 30 minutes. In the case of kinetic assay, substrate cleavage/product formation was monitored against 10, 15, 20, 25, 50, 100, 125, 150, 200, 250, 300, 350, 400, 500, 600, 700 nM of the RNA while reaction was quenched within the linear range of the time course curve (e.g. 1, 2, 3, etc. mins). RNA samples were thereafter mixed with loading dye (Thermo Fisher), heated at 95º C for 2 minutes and loaded onto 8% urea-PAGE gel. The gels were stained by SYBR® Gold (ThermoFisher) and reaction products were visualized under UV transilluminator (GeneSnap, Syngene). To quantify, intensity of the reaction products was calculated using GeneTools (Syngene) against a known amount of reference sample where purified 9S, p5S, and GlmZ RNAs were used as references to quantify the product/uncleaved substrate. Kinetics assay was performed for at least three time points (1, 2, 3, etc. mins) and each time point is a representative of technical duplicates. Next, reaction rate was plotted against substrate concentration using Prism (GraphPad Software).

ACKNOWLEDGEMENTS

The work was supported by a Wellcome Trust Investigator award to BFL (200873/Z/16/Z). For the purpose of open access, the author has applied a CC BY public copyright licence to any Author Accepted Manuscript version arising from this submission. We thank Tom Dendooven, Giulia Paris and Steven Hardwick for helpful suggestions and advice. We thank A.J. Carpousis (CNRS, Toulouse) for expression plasmids and discussions and Richard Cooley for advice about unnatural amino acid incorporation.

References

Agard NJ, Baskin JM, Prescher JA, Lo A, Bertozzi CR. 2006. A Comparative Study of Bioorthogonal Reactions with Azides. *ACS Chem Biol* **1**: 644–648. https://doi.org/10.1021/cb6003228.

Aït-Bara S, Carpousis AJ. 2015. RNA degradosomes in bacteria and chloroplasts: classification, distribution and evolution of RNase E homologs. *Mol Microbiol* **97**: 1021–1135. https://doi.org/10.1111/mmi.13095.

Aït-Bara S, Carpousis AJ, Quentin Y. 2015. RNase E in the γ-Proteobacteria: conservation of intrinsically disordered noncatalytic region and molecular evolution of microdomains. *Mol Genet Genomics* **290**: 847–862. https://doi.org/10.1007/s00438-014-0959-5.

Al-Husini N, Tomares DT, Bitar O, Childers WS, Schrader JM. 2018. α-Proteobacterial RNA Degradosomes Assemble Liquid-Liquid Phase-Separated RNP Bodies. *Mol Cell* **71**: 1027-1039.e14. https://www.sciencedirect.com/science/article/pii/S1097276518306373.

Al-Husini N, Tomares DT, Pfaffenberger ZJ, Muthunayake NS, Samad MA, Zuo T, Bitar O, Aretakis JR, Bharmal M-HM, Gega A, et al. 2020. BR-Bodies Provide Selectively Permeable Condensates that Stimulate mRNA Decay and Prevent Release of Decay Intermediates. *Mol Cell* **78**: 670-682.e8. https://www.sciencedirect.com/science/article/pii/S1097276520302276.

Baker KE, Mackie GA. 2003. Ectopic RNase E sites promote bypass of 5′-end-dependent mRNA decay in Escherichia coli. *Mol Microbiol* **47**: 75–88. https://doi.org/10.1046/j.1365-2958.2003.03292.x.

Bandyra KJ, Bouvier M, Carpousis AJ, Luisi BF. 2013. The social fabric of the RNA degradosome. *Biochim Biophys Acta - Gene Regul Mech* **1829**: 514–522. http://www.sciencedirect.com/science/article/pii/S1874939913000436.

Bandyra KJ, Wandzik JM, Luisi BF. 2018. Substrate Recognition and Autoinhibition in the Central Ribonuclease RNase E. *Mol Cell* **72**: 275-285.e4. http://www.sciencedirect.com/science/article/pii/S1097276518306993.

Boeynaems S, Alberti S, Fawzi NL, Mittag T, Polymenidou M, Rousseau F, Schymkowitz J, Shorter J, Wolozin B, Van Den Bosch L, et al. 2018. Protein Phase Separation: A New Phase in Cell Biology. *Trends Cell Biol* **28**: 420–435. https://www.sciencedirect.com/science/article/pii/S096289241830028X.

546 Bruce HA, Du D, Matak-Vinkovic D, Bandyra KJ, Broadhurst RW, Martin E, Sobott F,
547 Shkumatov A V, Luisi BF. 2018. Analysis of the natively unstructured RNA/protein-
548 recognition core in the Escherichia coli RNA degradosome and its interactions with
549 regulatory RNA/Hfq complexes. *Nucleic Acids Res* **46**: 387–402.
550 https://doi.org/10.1093/nar/gkx1083.

551 Callaghan AJ, Marcaida MJ, Stead JA, McDowall KJ, Scott WG, Luisi BF. 2005. Structure
552 of Escherichia coli RNase E catalytic domain and implications for RNA turnover.
553 *Nature* **437**: 1187–1191. https://doi.org/10.1038/nature04084.

554 Carlile TM, Rojas-Duran MF, Zinshteyn B, Shin H, Bartoli KM, Gilbert W V. 2014.
555 Pseudouridine profiling reveals regulated mRNA pseudouridylation in yeast and human
556 cells. *Nature* **515**: 143–146. https://doi.org/10.1038/nature13802.

557 Carpousis AJ, Van Houwe G, Ehretsmann C, Krisch HM. 1994. Copurification of E. coli
558 RNAase E and PNPase: Evidence for a specific association between two enzymes
559 important in RNA processing and degradation. *Cell* **76**: 889–900.
560 https://www.sciencedirect.com/science/article/pii/0092867494903638.

561 Chandran V, Poljak L, Vanzo NF, Leroy A, Miguel RN, Fernandez-Recio J, Parkinson J,
562 Burns C, Carpousis AJ, Luisi BF. 2007. Recognition and Cooperation Between the
563 ATP-dependent RNA Helicase RhlB and Ribonuclease RNase E. *J Mol Biol* **367**: 113–
564 132. https://www.sciencedirect.com/science/article/pii/S0022283606016731.

565 Chao Y, Li L, Girodat D, Förstner KU, Said N, Corcoran C, Śmiga M, Papenfort K,
566 Reinhardt R, Wieden H-J, et al. 2017. In Vivo Cleavage Map Illuminates the Central
567 Role of RNase E in Coding and Non-coding RNA Pathways. *Mol Cell* **65**: 39–51.
568 https://www.sciencedirect.com/science/article/pii/S1097276516307109.

569 Charette M, Gray MW. 2000. Pseudouridine in RNA: What, Where, How, and Why. *IUBMB*
570 *Life* **49**: 341–351. https://doi.org/10.1080/152165400410182.

571 Chatterjee D, Cooley RB, Boyd CD, Mehl RA, O'Toole GA, Sondermann H. 2014.
572 Mechanistic insight into the conserved allosteric regulation of periplasmic proteolysis by
573 the signaling molecule cyclic-di-GMP ed. J. Clardy. *Elife* **3**: e03650.
574 https://doi.org/10.7554/eLife.03650.

575 Christiansen J. 1988. The 9S RNA precursor of Escherichia coli 5S RNA has three structural
576 domains: implications for processing. *Nucleic Acids Res* **16**: 7457–7475.

https://doi.org/10.1093/nar/16.15.7457.

Clarke JE, Kime L, Romero A. D, McDowall KJ. 2014. Direct entry by RNase E is a major pathway for the degradation and processing of RNA in Escherichia coli. *Nucleic Acids Res* **42**: 11733–11751. https://doi.org/10.1093/nar/gku808.

Cormack RS, Mackie GA. 1992. Structural requirements for the processing of Escherichia coli 5 S ribosomal RNA by RNase E in vitro. *J Mol Biol* **228**: 1078–1090. http://www.sciencedirect.com/science/article/pii/002228369290316C.

Deana A, Belasco JG. 2005. Lost in translation: the influence of ribosomes on bacterial mRNA decay. *Genes Dev* **19**: 2526–2533. http://genesdev.cshlp.org/content/19/21/2526.abstract.

Del Campo C, Bartholomäus A, Fedyunin I, Ignatova Z. 2015. Secondary Structure across the Bacterial Transcriptome Reveals Versatile Roles in mRNA Regulation and Function. *PLOS Genet* **11**: e1005613. https://doi.org/10.1371/journal.pgen.1005613.

Dendooven, T, Sinha, D, Roeselova, A, Cameron, TA, De Lay NR, Luisi, BF, Bandyra KJ. 2021. A cooperative PNPase-Hfq-RNA carrier complex facilitates bacterial riboregulation. *Mol Cell* **81**, 2901-2913.

Dreyfus MBT-P in MB and TS. 2009. Chapter 11 Killer and Protective Ribosomes. In *Molecular Biology of RNA Processing and Decay in Prokaryotes*, Vol. 85 of, pp. 423–466, Academic Press https://www.sciencedirect.com/science/article/pii/S0079660308008118.

Durica-Mitic S, Görke B. 2019. Feedback regulation of small RNA processing by the cleavage product. *RNA Biol* **16**: 1055–1065. https://doi.org/10.1080/15476286.2019.1612693.

Garrey SM, Blech M, Riffell JL, Hankins JS, Stickney LM, Diver M, Hsu Y-HR, Kunanithy V, Mackie GA. 2009. Substrate Binding and Active Site Residues in RNases E and G. *J Biol Chem* **284**: 31843–31850. https://www.sciencedirect.com/science/article/pii/S002192582037931X.

Gonzalez GM, Durica-Mitic S, Hardwick SW, Moncrieffe MC, Resch M, Neumann P, Ficner R, Görke B, Luisi BF. 2017. Structural insights into RapZ-mediated regulation of bacterial amino-sugar metabolism. *Nucleic Acids Res* **45**: 10845–10860. https://doi.org/10.1093/nar/gkx732.

608 Göpel Y, Papenfort K, Reichenbach B, Vogel J, Görke B. 2013. Targeted decay of a
609 regulatory small RNA by an adaptor protein for RNase E and counteraction by an anti-
610 adaptor RNA. *Genes Dev* **27**: 552–564. http://europepmc.org/abstract/MED/23475961.

611 Guzikowski AR, Chen YS, Zid BM. 2019. Stress-induced mRNP granules: Form and
612 function of processing bodies and stress granules. *WIREs RNA* **10**: e1524.
613 https://doi.org/10.1002/wrna.1524.

614 Guzzi N, Cieśla M, Ngoc PCT, Lang S, Arora S, Dimitriou M, Pimková K, Sommarin MNE,
615 Munita R, Lubas M, et al. 2018. Pseudouridylation of tRNA-Derived Fragments Steers
616 Translational Control in Stem Cells. *Cell* **173**: 1204-1216.e26.
617 https://www.sciencedirect.com/science/article/pii/S0092867418302885.

618 Hadjeras L, Poljak L, Bouvier M, Morin-Ogier Q, Canal I, Cocaign-Bousquet M, Girbal L,
619 Carpousis AJ. 2019. Detachment of the RNA degradosome from the inner membrane of
620 Escherichia coli results in a global slowdown of mRNA degradation, proteolysis of
621 RNase E and increased turnover of ribosome-free transcripts. *Mol Microbiol* **111**: 1715–
622 1731. https://doi.org/10.1111/mmi.14248.

623 Kalamorz F, Reichenbach B, März W, Rak B, Görke B. 2007. Feedback control of
624 glucosamine-6-phosphate synthase GlmS expression depends on the small RNA GlmZ
625 and involves the novel protein YhbJ in Escherichia coli. *Mol Microbiol* **65**: 1518–1533.
626 https://doi.org/10.1111/j.1365-2958.2007.05888.x.

627 Khemici V, Carpousis AJ. 2004. The RNA degradosome and poly(A) polymerase of
628 Escherichia coli are required in vivo for the degradation of small mRNA decay
629 intermediates containing REP-stabilizers. *Mol Microbiol* **51**: 777–790.
630 https://doi.org/10.1046/j.1365-2958.2003.03862.x.

631 Kime L, Clarke JE, Romero A. D, Grasby JA, McDowall KJ. 2014. Adjacent single-stranded
632 regions mediate processing of tRNA precursors by RNase E direct entry. *Nucleic Acids*
633 *Res* **42**: 4577–4589. https://doi.org/10.1093/nar/gkt1403.

634 Kime L, Jourdan SS, Stead JA, Hidalgo-Sastre A, McDowall KJ. 2010. Rapid cleavage of
635 RNA by RNase E in the absence of 5′ monophosphate stimulation. *Mol Microbiol* **76**:
636 590–604. https://doi.org/10.1111/j.1365-2958.2009.06935.x.

637 Koslover DJ, Callaghan AJ, Marcaida MJ, Garman EF, Martick M, Scott WG, Luisi BF.
638 2008. The Crystal Structure of the Escherichia coli RNase E Apoprotein and a

Mechanism for RNA Degradation. *Structure* **16**: 1238–1244. https://www.sciencedirect.com/science/article/pii/S0969212608002530.

Leroy A, Vanzo NF, Sousa S, Dreyfus M, Carpousis AJ. 2002. Function in Escherichia coli of the non-catalytic part of RNase E: role in the degradation of ribosome-free mRNA. *Mol Microbiol* **45**: 1231–1243. https://doi.org/10.1046/j.1365-2958.2002.03104.x.

Lin Y, Protter DSW, Rosen MK, Parker R. 2015. Formation and Maturation of Phase-Separated Liquid Droplets by RNA-Binding Proteins. *Mol Cell* **60**: 208–219. https://www.sciencedirect.com/science/article/pii/S1097276515006644.

Lorenz R, Bernhart SH, Höner zu Siederdissen C, Tafer H, Flamm C, Stadler PF, Hofacker IL. 2011. ViennaRNA Package 2.0. *Algorithms Mol Biol* **6**: 26. https://doi.org/10.1186/1748-7188-6-26.

Mackie GA. 1998. Ribonuclease E is a 5′-end-dependent endonuclease. *Nature* **395**: 720–724. https://doi.org/10.1038/27246.

Mackie GA. 2013. RNase E: at the interface of bacterial RNA processing and decay. *Nat Rev Microbiol* **11**: 45–57. https://doi.org/10.1038/nrmicro2930.

Mackie GA, Genereaux JL. 1993. The Role of RNA Structure in Determining RNase E-dependent Cleavage Sites in the mRNA for Ribosomal Protein S20 in vitro. *J Mol Biol* **234**: 998–1012. https://www.sciencedirect.com/science/article/pii/S0022283683716542.

Marcaida MJ, DePristo MA, Chandran V, Carpousis AJ, Luisi BF. 2006. The RNA degradosome: life in the fast lane of adaptive molecular evolution. *Trends Biochem Sci* **31**: 359–365. https://doi.org/10.1016/j.tibs.2006.05.005.

Moffitt JR, Pandey S, Boettiger AN, Wang S, Zhuang X. 2016. Spatial organization shapes the turnover of a bacterial transcriptome ed. R. Green. *Elife* **5**: e13065. https://doi.org/10.7554/eLife.13065.

Nott TJ, Petsalaki E, Farber P, Jervis D, Fussner E, Plochowietz A, Craggs TD, Bazett-Jones DP, Pawson T, Forman-Kay JD, et al. 2015. Phase Transition of a Disordered Nuage Protein Generates Environmentally Responsive Membraneless Organelles. *Mol Cell* **57**: 936–947. https://www.sciencedirect.com/science/article/pii/S1097276515000143.

Pereira J, Lupas AN. 2018. The ancestral KH peptide at the root of a domain family with three different folds. *Bioinformatics* **34**: 3961–3965. https://doi.org/10.1093/bioinformatics/bty480.

Richards J, Belasco JG. 2021. Widespread Protection of RNA Cleavage Sites by a Riboswitch Aptamer that Folds as a Compact Obstacle to Scanning by RNase E. *Mol Cell* **81**: 127-138.e4. https://www.sciencedirect.com/science/article/pii/S1097276520307322.

Saxon E, Bertozzi CR. 2000. Cell Surface Engineering by a Modified Staudinger Reaction. *Science (80-)* **287**: 2007 LP – 2010. http://science.sciencemag.org/content/287/5460/2007.abstract.

Strahl H, Turlan C, Khalid S, Bond PJ, Kebalo J-M, Peyron P, Poljak L, Bouvier M, Hamoen L, Luisi BF, et al. 2015. Membrane Recognition and Dynamics of the RNA Degradosome. *PLOS Genet* **11**: e1004961. https://doi.org/10.1371/journal.pgen.1004961.

Sulthana S, Basturea GN, Deutscher MP. 2016. Elucidation of pathways of ribosomal RNA degradation: an essential role for RNase E. *RNA* **22**: 1163–1171. http://rnajournal.cshlp.org/content/22/8/1163.abstract.

Thompson KJ, Zong J, Mackie GA. 2015. Altering the Divalent Metal Ion Preference of RNase E ed. R.L. Gourse. *J Bacteriol* **197**: 477 LP – 482. http://jb.asm.org/content/197/3/477.abstract.

Tsai Y-C, Du D, Domínguez-Malfavón L, Dimastrogiovanni D, Cross J, Callaghan AJ, García-Mena J, Luisi BF. 2012. Recognition of the 70S ribosome and polysome by the RNA degradosome in Escherichia coli. *Nucleic Acids Res* **40**: 10417–10431. https://doi.org/10.1093/nar/gks739.

Updegrove TB, Kouse AB, Bandyra KJ, Storz G. 2019. Stem-loops direct precise processing of 3′ UTR-derived small RNA MicL. *Nucleic Acids Res* **47**: 1482–1492. https://doi.org/10.1093/nar/gky1175.

Urban JH, Vogel J. 2008. Two Seemingly Homologous Noncoding RNAs Act Hierarchically to Activate glmS mRNA Translation. *PLOS Biol* **6**: e64. https://doi.org/10.1371/journal.pbio.0060064.

Westhof E. 2019. Pseudouridines or how to draw on weak energy differences. *Biochem Biophys Res Commun* **520**: 702–704. https://www.sciencedirect.com/science/article/pii/S0006291X19318984.

701

Table 1. Kinetics parameters for RNA cleavage catalyzed by RNase E catalytic domain and the degradosome assembly*

Enzyme	**Concentration (nM)**	**RNA substrate****	**Substrate Degradation /Product Formation (%)+**	**V_{max} (nM.s^{-1})**	**K_m(nM)**	**k_{cat} (s^{-1}) (10^{-4})**	**k_{cat}/K_m (s^{-1}. nM^{-1})*****
NTD	125	5′PPP-9S	95.5/28.6	0.90	75.4 ±11.9	72.3±3.2	9.5 ± (1.5) x 10^{-5}
		5′P-9S	95.6/36.3	1.44	85.8±9.4	115.5±4.0	13.4 ± (1.5) x 10^{-5}
		5′PPP-GlmZ	97.5/ND	4.81	521.4±75.2	384.9±33	7.2 ± (1.2) x 10^{-5}
NTD-3M	125	5′PPP-9S	97.3/41.1	1.38	41.8±6.8	110.9±4.3	26.5 ± (4.4) x 10^{-5}
		5′P-9S	98.0/48.2	2.87	96.9±9.7	229.6±7.1	23.5 ± (2.5) x 10^{-5}
		5′PPP-GlmZ	99.4/ND	11.68	729.0±100.5	934.5±82.1	12.7 ± (2.0) x 10^{-5}
Truncated degradosome	50	5′PPP-9S	99.6/45.2	1.05	61.1±8.1	210.5±7.2	34.3 ± (4.7) x 10^{-5}
		5′P-9S	100/62.3	2.26	116.3±12.7	453.7±16.4	38.9 ± (4.5) x 10^{-5}
		5′PPP-GlmZ	100/ND	7.02	545.3±90.5	1404.0±135.2	25.6 ± (4.9) x 10^{-5}
Full degradosome	25	5′PPP-9S	99.6/51.9	2.1	95.3±9.4	839.9±29.2	88.0 ± (9.2) x 10^{-5}
		5′P-9S	100/63.8	2.32	121.1±15.0	931.6±40.3	83.7 ±(11.0) x 10^{-5}
		5′PPP-GlmZ	100/ND	7.15	679.2±118.8	2863.0±308.9	42.1 ± (8.7) x 10^{-5}

*The results are from triplicates and the errors are standard deviation of the mean.

**5′PPP = 5′-triphosphate, 5′P =5′-monophosphate +ND – not determined. ***Estimated from errors for *Km* and k_{cat}

706 **Table 2. Primers for inserting conditional stop codons (TAG) in RNase E**

707

M130STOP Forward: 5′-GTAGCTATCTGG TTCTGTAGCCGAACAACCCGCGCGCGGGTGG-3′ Reverse: 5′-CCACCCGCGCGCGGGTTGTTCGGCTACAGAACCAGATAGCTAC-3′
I139STOP Forward: 5′-CAACCCGCGCGCGGGTGGCTAGTCTCGCCGTATCGAAGGCGACG-3′ Reverse: 5′-CGTCGCCTTCGATACGGCGAGACTAGCCACCCGCGCGCGGGTTG-3′
R142STOP Forward: 5′-GCGGGTGGCATTTCTCGCTAGATCGAAGGCGACGACCGTACCG-3′ Reverse: 5′-CGGTACGGTCGTCGCCTTCGATCTAGCGAGAAATGCCACCCGC-3′
Y269STOP Forward: 5′-GTTCAGCCACTAGCAGATCGAGTCACAG-3′ Reverse: 5′-CTGTGACTCGATCTGCTAGTGGCTGAAC-3′

708

709

710

Figure Legends

Figure 1. Role of RNase E K112 in interaction with uracil +2 of the substrate, and impact of pseudouridylation. (a) The tetrameric RNase E catalytic domain (NTD) in complex with RNA (PDB: 2C0B) (Callaghan et al. 2005). The inset on the upper right shows a cartoon schematic of the domains showing active-site residues D303 and D346. The lower inset shows a model of the organisation of binding of RNA substrate based on the structure of chemically protected RNA (PDB 2C0B). The residues in purple are from the S1 domain of RNase E and the scissile phosphate from the RNA bound in the active site on the interface of two protomers presented for the hydrolytic attack by the waters associated (W, red) with magnesium ion (Mg^{++}, green sphere); the U+2 is proposed to be sandwiched between side chains of amino acids K112 and F67. (b) Cleavage assays of RNase E. Cleavage of 20-mer poly-adenine (A20), poly-adenine with an uracil at position 15 (A20U), and poly-adenine with a pseudouridine (Ψ) at position 15 (A20Ψ) by wild-type RNase E NTD (top panel), RNase E NTD with a mutation of K112A (middle panel) and K112Q (bottom panel). The substrate was 5′ end-labelled and the products were resolved on a denaturing urea-PAGE gels. The time points of the reactions are annotated above the gels. (c) A proposed model of the likely hydration organisation at the site of pseudouridine (Ψ). The model also shows a probable hydrogen-bond mediated interaction between K112 and pseudouridine. A crystal structure of a duplex RNA (PDB 3CGS) was used to make the model.

Figure 2. Mutations in the RNase H-like and DNase I domains improve catalytic efficiency of RNase E. (a) The left shows a schematic of secondary structure of 9S RNA with three cleavage sites marked as "*a*", "*b*", and "*c*" (Lorenz et al. 2011; Christiansen 1988); the bars above the schematic show the three segments (9S-V1, 9S-V2, and 9S-V3) generated for cleavage assays. The middle panel shows secondary structure of GlmZ RNA predicted by the ViennaRNA Package 2.0 (Lorenz et al. 2011).The right panel shows an annotated domain schematic for NTD-wt and NTD-3M harboring mutations in RNase H-like (D26N and D28N) and DNase I (D338N) domains. (b) Denaturing RNA gels showing

time course cleavage assay of 9S (5′-triphosphorylated, upper panel; 5′-monophosphorylated, lower panel) using NTD-wt (blue lines) and the NTD-3M (red lines). The lower panel shows the integrated signal for 9S (left) and p5S product (right). (c) Integrated signal for the 9S segments V1, V2 and V3 obtained against NTD-wt and NTD-3M. (d) Integrated signal for GlmZ cleavage over time for NTD-wt and NTD-3M shown on the left panel with the corresponding denaturing gels shown on the right. (e) Denaturing RNA gels for GlmZ processing by NTD-wt and NTD-3M in the presence of RapZ or Hfq, showing the production of GlmZ-Pro is sensitive to the presence of RapZ but not Hfq. (f) Michaelis-Menten plots used to determine the kinetics parameters of cleavage of 9S and GlmZ RNAs. The plots were fitted using Prism (GraphPad Software) and represent mean of three representative plots of reaction rates *vs* substrate concentrations (see "Materials and Methods" for details). H = RNase H-like domain, S1 = RNA binding S1 domain, DNase I = DNase I-like domain, 5′ = RNA 5′ site-sensing pocket, Zn = Zn-linker.

Figure 3. Metal interactions in the active site of RNase E. (a) Schematic of RNase E NTD showing mutant D346C in the active site. The mutant is catalytically active in presence of Mn^{++} but not any other metal as seen for processing of 9S and sRNA RprA (b,c, respectively). (d) An isothermal calorimetry titration curve for NTD.D346C interactions with Mn^{++}. The K_D is 17 μM for Mn^{++}. The titration curve is representative of three independent experiments.

Figure 4. Incorporation of azido-phenylalanine into the RNase E catalytic domain. (a) Chemical formula of para-azido-phenylalanine (p-AzidoPhe); inset shows p-AzidoPhe photo-crosslinking to nearby residues upon exposure to UV light at 254 nm. (b) Models of RNase E NTD tetramer with bound RNA at active site, 5′ sensor and the duplex recognition region with insets showing the residues (M130, I139, R142, and Y269) substituted with p-AzidoPhe (model based on PDB 2C0B). (c) Time course assay of p5S production from 9S RNA, processed by p-AzidoPhe derivatives of NTD; values represent mean (n = 3) and standard deviation. (d) Denaturing protein gels showing p-AzidoPhe derivatives of

RNase E NTD form cross-linked product(s). The p-AzidoPhe modified protein may form intra-domain interaction(s) upon light exposure which are lost in the presence of 9S RNA, suggesting masking of the crosslinking moiety upon RNA binding.

Figure 5. Substrate cleavage catalyzed by the RNA degradosome complex. (a) Schematics of the full degradosome (RNase E, enolase, RhlB, and PNPase) and truncated degradosome (RNase E, enolase, and RhlB) assemblies. (b) Time course cleavage assay showing processing of 9S RNA and production of the precursor RNA p5S for 9S RNA with 5′-triphosphate (PPP-9S, upper panel) and 5′-monophosphate (P-9S, middle panel). The lower panel shows integrated signal for 9S signal loss (plot on the left) and p5S signal gain (plot on the right) from 9S cleavage assays catalyzed by truncated degradosome (green lines) and full degradosome (orange lines). (c) Plots of cleavage of 9S subdomains (9S-V1, 9S-V2, and 9S-V3) catalyzed by degradosome assemblies. (d) Plots of cleavage of GlmZ RNA catalyzed by the degradosome assemblies with the denaturing gels used to quantify signals shown on the right. (e) Denaturing gels showing the production of GlmZ-Pro by RNase E is sensitive to the presence of RapZ but not Hfq within the degradosome assembly too. (f) Michaelis-Menten plots used for determination of the kinetics parameters of the cleavage of 9S and GlmZ RNAs catalyzed by truncated degradosome and full degradosome. The plots were fitted using Prism (GraphPad Software) and represent mean of three representative plots of reaction rates *vs* substrate concentrations (see "Materials and Methods" for details). H = RNase H-like domain, S1 = RNA binding S1 domain, DNase I = DNase I-like domain, 5′ = RNA 5′ site-sensing pocket, Zn = Zn-linker, MTS = membrane targeting site, AR = Arginine-rich region/RNA binding site, HBS = RhlB binding site, EBS = Enolase binding site, and PBS = PNPase binding site.

Figure 6. Proposed model for substrate recognition and processing by RNase E. RNase E mediated processing of RNAs within the degradosome assembly is sensitive to substrate entry and product exit where other degradosome proteins RhlB, Enolase, and PNPase play an important role. The

789 endonuclease activity of RNase E is guided by side chain interaction with substrate and geometrical
790 details including hydration pattern that can be influenced by pseudouridine substitution.

791

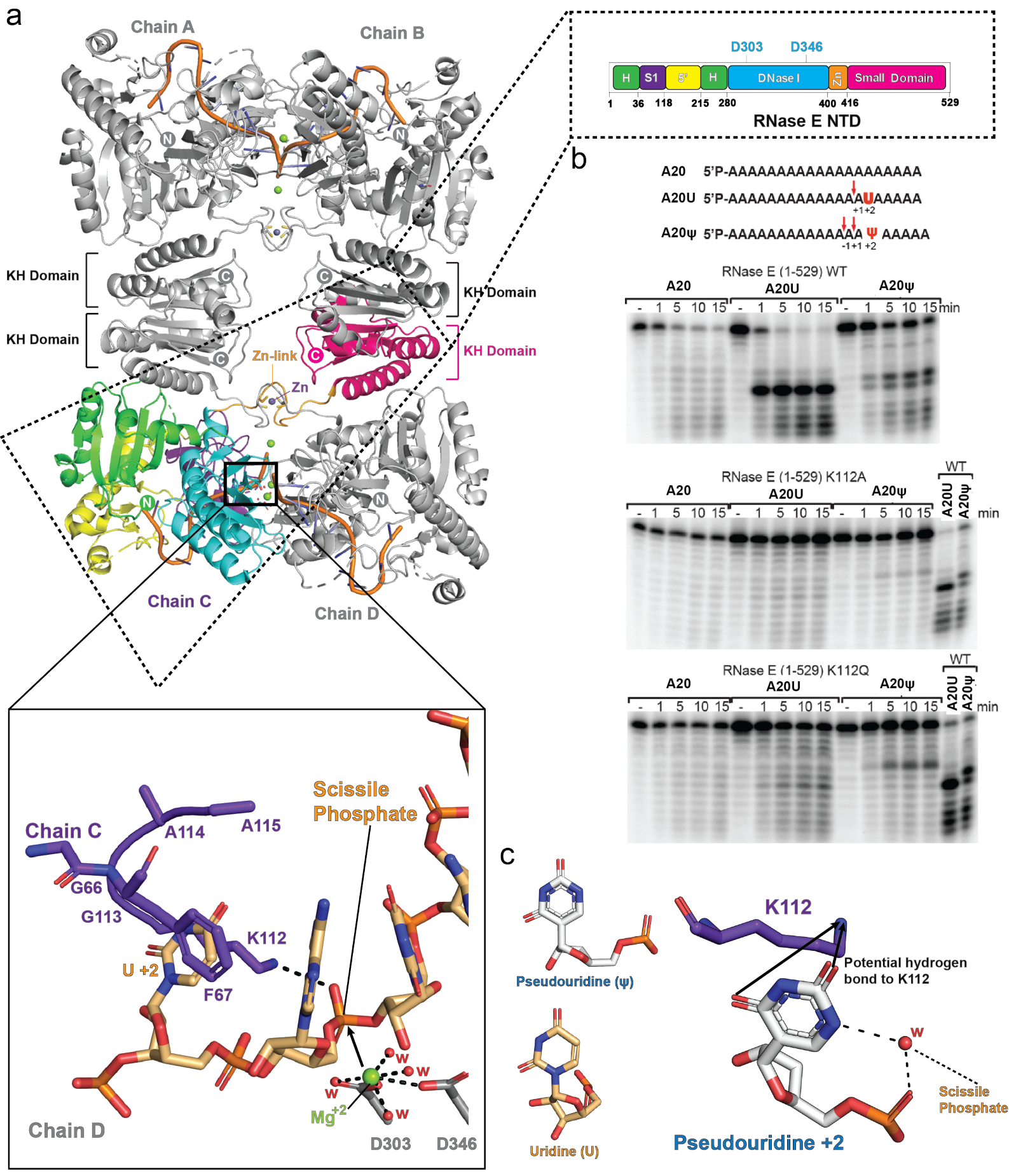

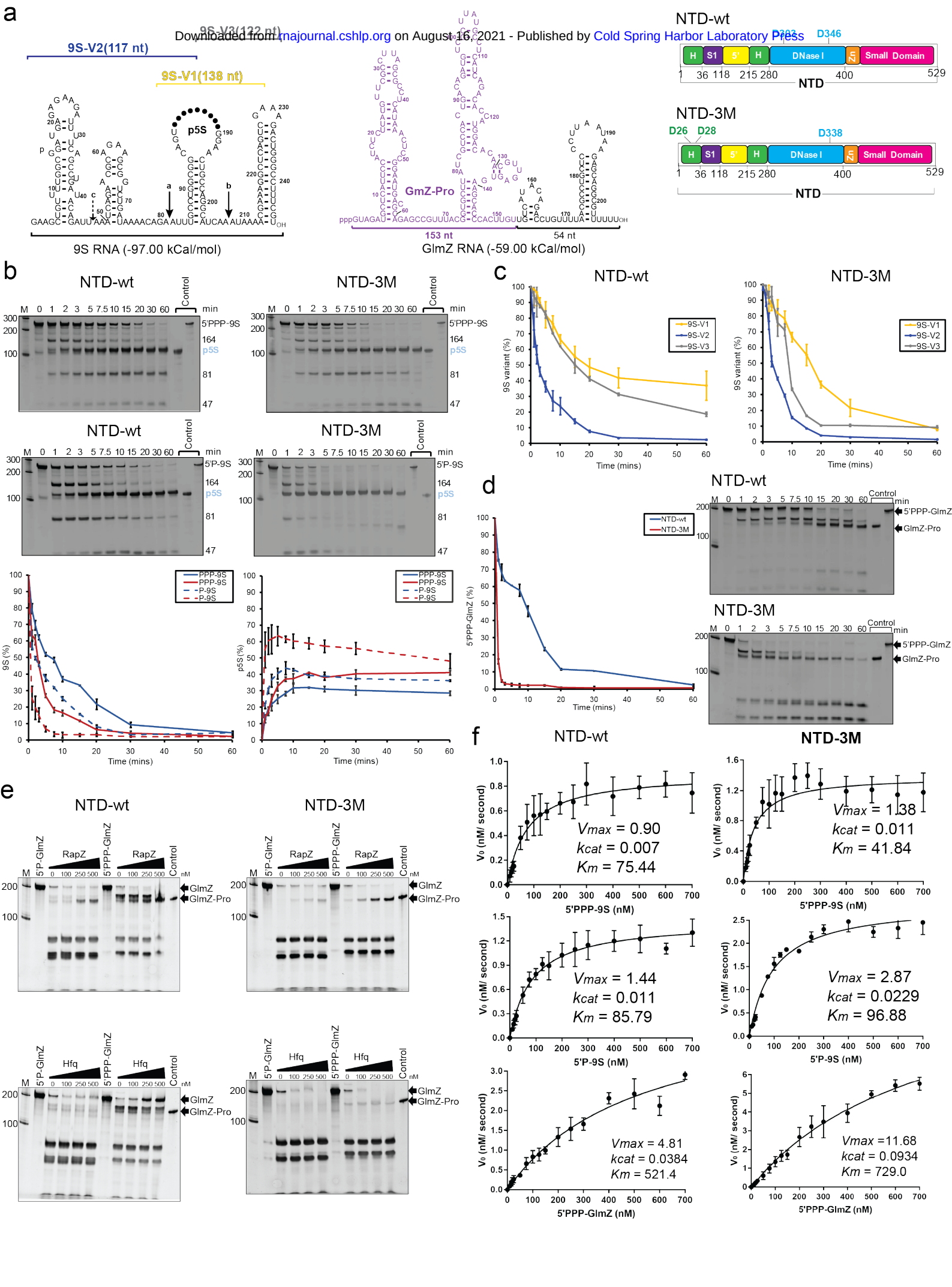

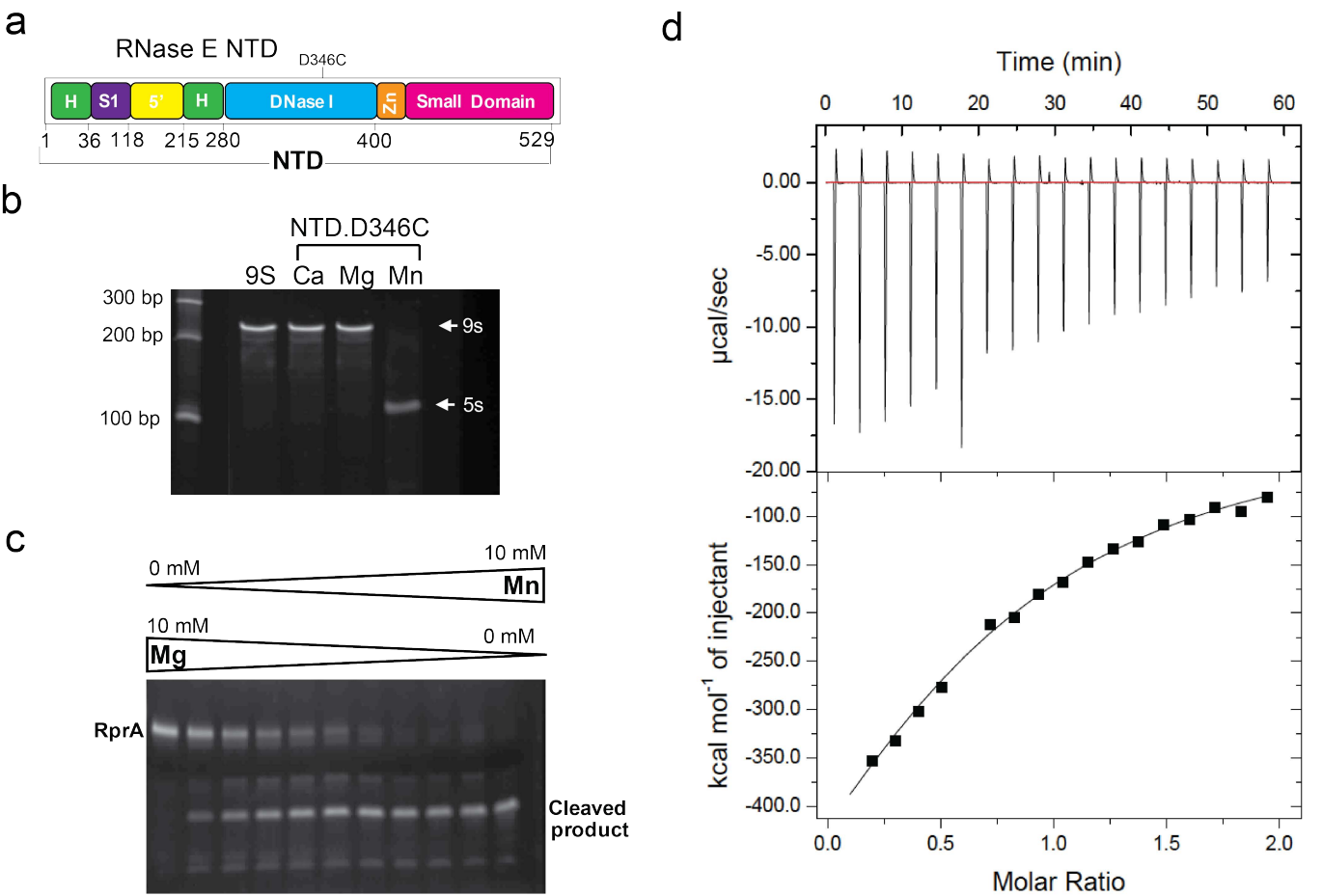
a
RNase E NTD
D346C
H
S1
5'
H
DNase I
Zn
Small Domain
1
36
118
215
280
400
529
NTD
b
NTD.D346C
9S
Ca
Mg
Mn
300 bp
200 bp
100 bp
9s
5s
c
0 mM
10 mM
Mn
10 mM
0 mM
Mg
RprA
Cleaved product
d
Time (min)
0
10
20
30
40
50
60
µcal/sec
0.00
-5.00
-10.00
-15.00
-20.00
kcal mol-1 of injectant
-100.0
-150.0
-200.0
-250.0
-300.0
-350.0
-400.0
0.0
0.5
1.0
1.5
2.0
Molar Ratio

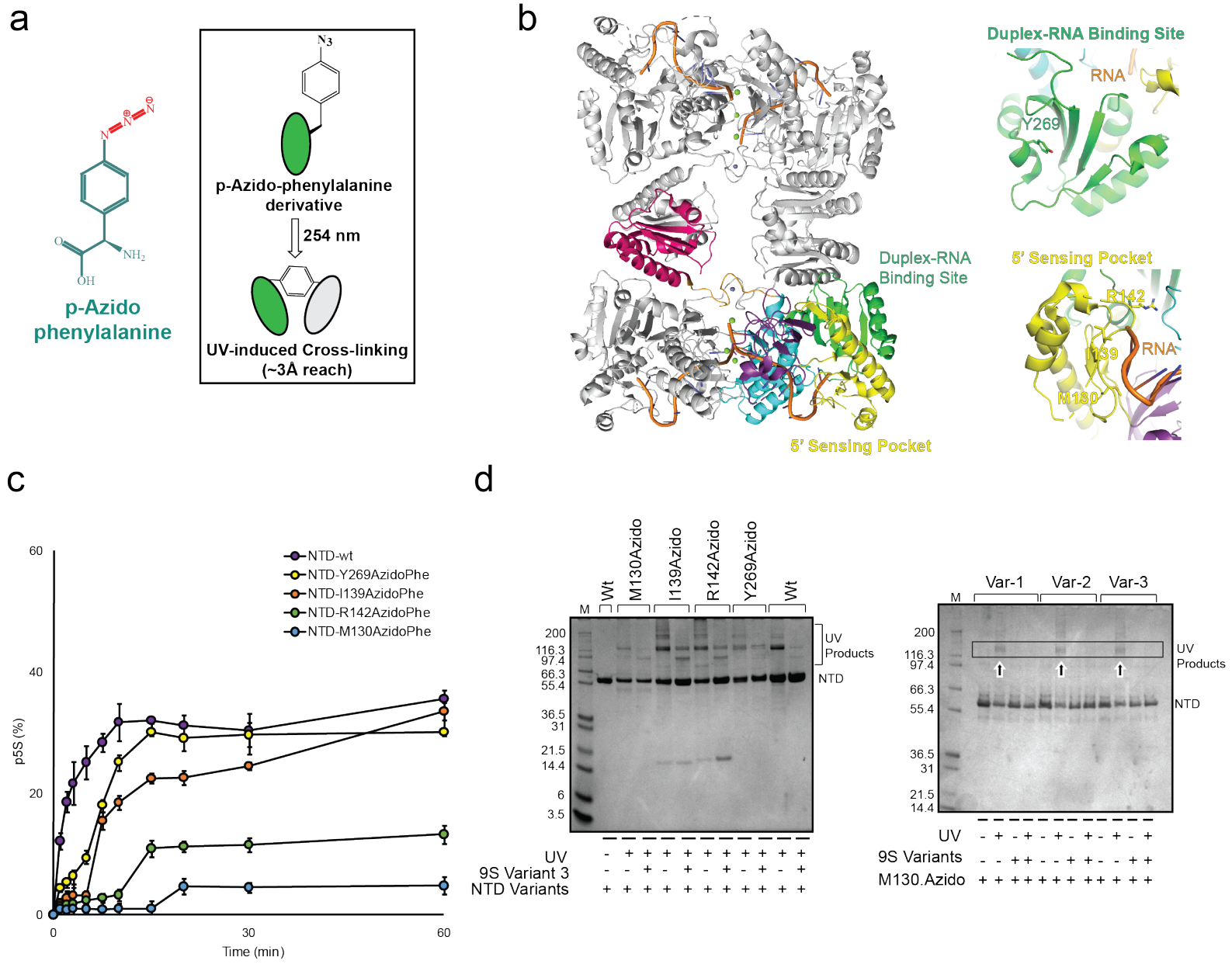

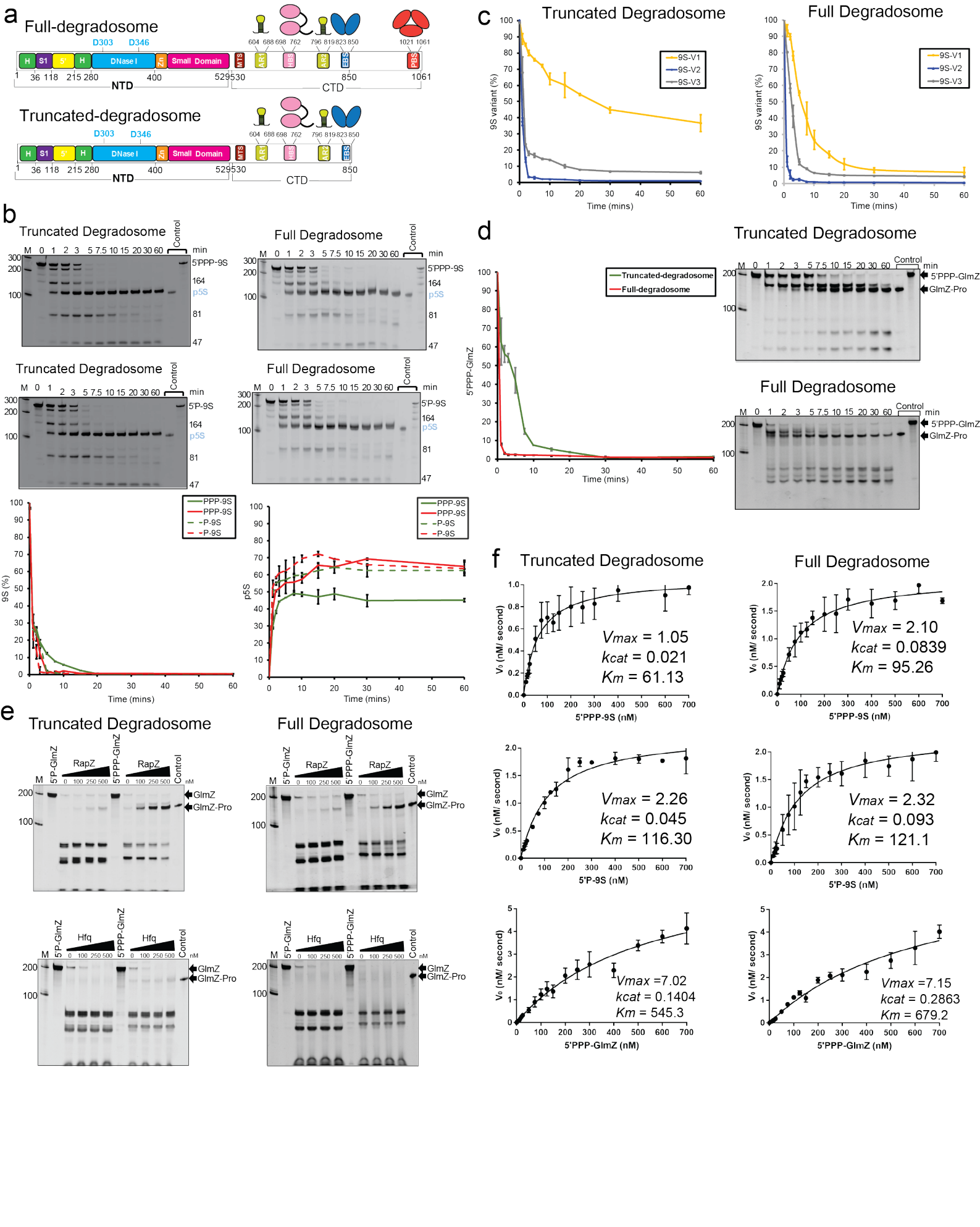

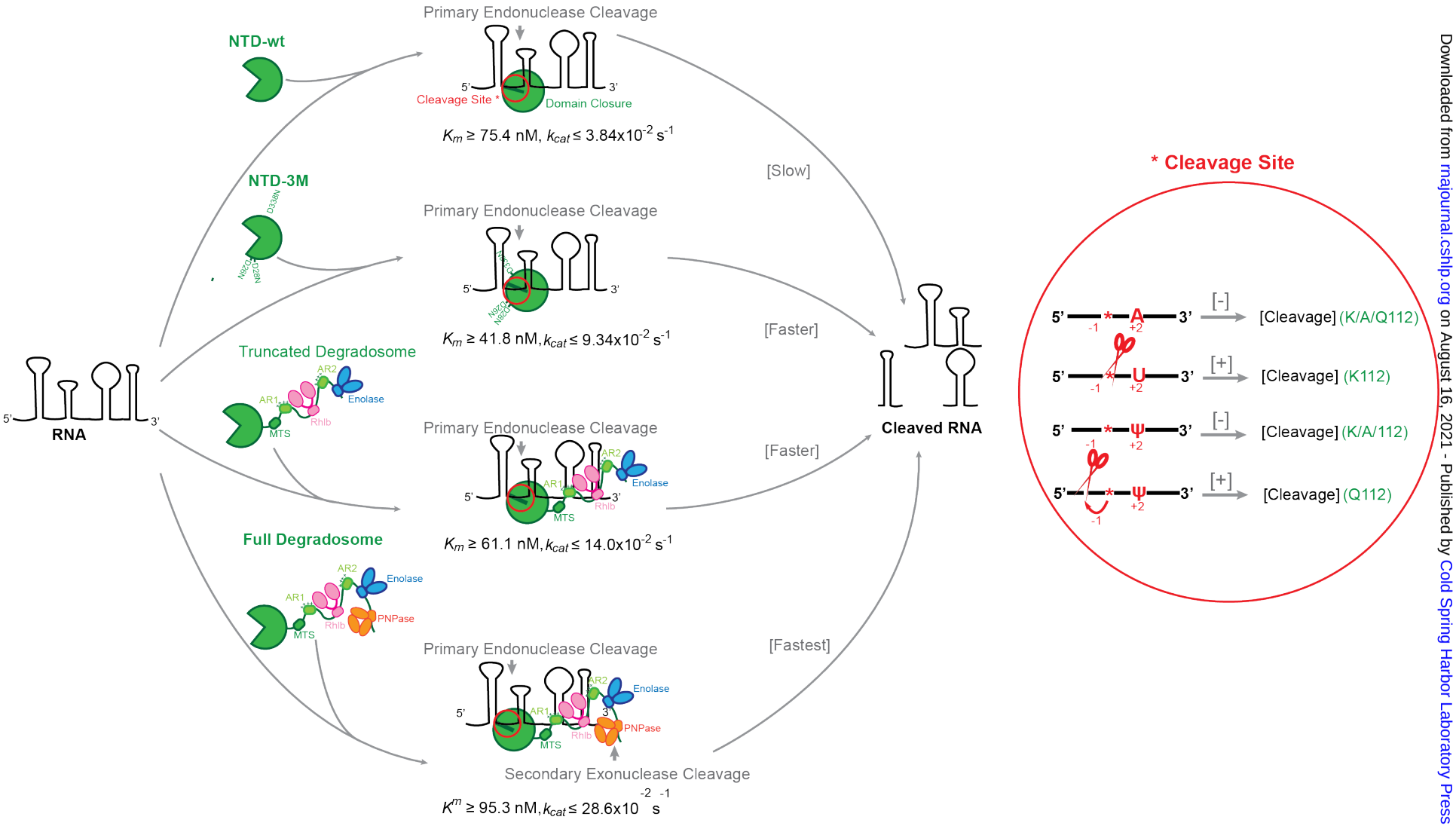

Impact of pseudo-uridylation, substrate fold and degradosome organization on the endonuclease activity of RNase E

M Saiful Islam, Katarzyna J Bandyra, Yanjie Chao, et al.

RNA published online August 2, 2021